

Investigation of Ni catalyst activation during plasma-assisted methane oxidation

Yudong Li, Michael Hinshelwood, and Gottlieb S. Oehrlein*

Department of Materials Science and Engineering and the Institute for Research in Electronics and Applied Physics, University of Maryland, College Park, MD 20742, USA

*Corresponding author: oehrlein@umd.edu

Abstract

Atmospheric pressure plasma has shown promise in improving thermally activated catalytic reactions through a process termed plasma-catalysis synergy. In this work, we investigated atmospheric pressure plasma jet (APPJ)-assisted CH₄ oxidation over a Ni/SiO₂/Al₂O₃ catalyst. Downstream gas-phase products from CH₄ conversion were quantified by Fourier transform infrared spectroscopy (FTIR). The catalyst near-surface region was characterized by in-situ diffuse reflectance infrared Fourier transform spectroscopy (DRIFTS). The catalyst was observed to be activated at elevated temperature (500 °C) if it was exposed to the APPJ operated at large plasma power. “Catalyst activation” signifies that the purely thermal conversion of CH₄ using catalysts which had been pre-exposed to plasma became more intense and produced consistently CO product, even if the plasma was extinguished. Without the application of the APPJ to the Ni catalyst surface this was not observed at 500 °C. The study of different exposure conditions of the activated catalyst indicates that the reduction of the catalyst by the APPJ is likely the cause of the catalyst activation. We also observed a systematic shift of the vibrational frequency of adsorbed CO on Ni catalyst when plasma operating conditions and catalyst temperatures were varied and discussed possible explanations for the observed changes. This work provides insights into the plasma-catalyst interaction, especially catalyst modification in the plasma catalysis process, and potentially demonstrates the possibility of utilizing the surface CO as a local probe to understand the plasma-catalyst interaction and shed light on the complexity of plasma catalysis.

1. Introduction

Atmospheric pressure plasmas produce reactive species, such as neutrals, ions, electrons, and photons, which can be applied in material processing [1], waste treatment [2], surface decontamination [3], and catalysis [4]. Plasma-catalysis is a growing field that has shown potential to improve conventional thermally-driven catalytic reactions, including ammonia synthesis [5], CO₂ reduction [6], hydrocarbon reforming [7], and others.

Syngas with a lower H₂/CO ratio is beneficial for the synthesis of valuable oxygenate chemicals like methanol [8]. Compared to dry reforming and water reforming of methane, the partial oxidation of methane to syngas is an exothermal process and the energy utilization is more efficient [9]. The main products of partial oxidation reactions of CH₄ are CO, CO₂, H₂O and H₂ [9]. The mechanism and reaction pathways of partial oxidation of CH₄ still remains unclear [10, 11]. For instance, researchers have not reached an agreement on whether the primary product is CO or CO₂. Two reaction mechanisms are widely considered: (i) CH₄ is broken down to CH_n, which is further oxidized to CO and CO₂ over the catalyst [12]; (ii) CH₄ undergoes combustion with O₂ over the catalyst to CO₂. Subsequently, the generated CO₂ is reformed with CH₄ to produce CO [11].

Compared to the tremendous effort invested in the investigation of conversion rates and selectivity among different catalysts, fundamental research on the mechanism of plasma catalysis has drawn less attention. One of the difficulties is the lack of clear understanding of the thermal catalytic reaction pathways, as illustrated above the example of methane partial oxidation. The addition of plasma to the system increases complexity by increasing possible

reaction pathways, and thus reaction mechanism(s) become more complex as thermal reactions and additional plasma induced effects start to interact [13]. Another obstacle is the difficulty to implement in-situ surface characterization. The plasma source usually physically contacts the catalyst, e.g. in a packed bed dielectric barrier discharge system [14], and thus makes the system difficult to be probed by surface characterization techniques. Moreover, the plasma-assisted catalytic reactions take place at high pressure, e.g., atmospheric pressure, which precludes the application of many standard surface characterization techniques that require a vacuum environment. The lack of surface characterization data and information on surface species is a major limitation for clarifying and distinguishing reaction pathways.

The plasma-catalyst coupling usually results in synergistic effects that are reflected by an enhancement of reactions, e.g. improvement of the product yield [14] or a reduction of activation energy [15]. The plasma-catalysis synergy effect is thought to result from three aspects: (i) Plasma-produced reactive species are transported to the catalyst surface and enhance the surface reaction rates [13]; (ii) High-energy plasma-produced species activate stable reactants, e.g. dehydrogenation of CH_4 to CH_n takes place, and the more reactive species interact with the catalyst surface with a lower energy barrier [15]; (iii) Plasma directly induces reactions in the plasma gas phase [16]. In addition, plasma can modify the catalyst surface, e.g., change the surface composition and morphology [17-20], which may be responsible for plasma-catalyst synergy. The reactive plasma-produced species are found to inhibit inert adsorbates on surface, such as coke formation in CH_4 reforming [21] and N atoms in ammonia synthesis [22], hence active catalyst sites can be exposed to the reactants and sustain the reactions. The plasma can also modify catalysts by altering their electronic properties [23], selectively doping

atoms or modifying the bandgap of the catalyst [4]. These plasma-induced modifications might lead to a change of the overall catalytic performance. Nevertheless, due to the lack of enough fundamental research on plasma-catalyst interactions, the nature of the catalyst modifications, and how such modifications may be related to plasma-catalyst synergy or coupling remain unknown [24].

In this work, we investigated CH₄/O₂/Ar APPJ-assisted CH₄ oxidation over a nickel catalyst on SiO₂/Al₂O₃ support. The catalyst was observed to be activated when the plasma source was operated using relatively large power levels. The catalyst characterization data obtained here indicate that this catalyst activation may be related to the reduction of the catalyst by plasma-produced species. We also observed a systematic shift of CO vibrational frequency with plasma operating conditions and catalyst temperature. These observations may provide a new perspective for understanding the mechanism of plasma catalysis for the current system and which processes may be responsible for observed plasma-catalysis synergy.

2. Experimental setup and catalyst material

The experimental setup is illustrated in figure 1. The APPJ was integrated in a reactor that enables real-time gas phase and operando surface characterizations. This setup has been developed in the past few years and a detailed description of the setup can be found in [25, 26].

2.1 Plasma source and catalyst

The plasma source used in this work was a RF plasma jet driven at 14.3 MHz, with 20 kHz modulation and a 20% on and 80% off duty cycle to dissipate heat. A high voltage tungsten pin was placed in the center of a dielectric quartz tube with a grounded ring electrode attached at

the end of it. Upon ignition, the plasma was generated at the tip of the tungsten pin and the plasma-produced species were transported to the catalyst bed where the plasma-catalyst interaction took place. The plasma feed gas used in this study was 2 sccm CH₄ and 1 sccm O₂ carried by 200 sccm Ar, while 400 sccm Ar was flown to the reactor chamber and downstream of the plasma to dissipate heat and keep the gas residence time consistent with prior work [25, 26]. In previous work, we studied O₂/Ar plasma, while CH₄/Ar was flown downstream of the plasma into the chamber and interacted with the plasma-produced species on the catalyst surface. The catalyst material was an unreduced nickel powder catalyst supported by Al₂O₃ (13 wt%) and SiO₂ (12 wt%). Temperature of the catalyst was controlled by a heating plate and a thermometer inserted at the bottom of the catalyst bed. It is worth noting that the generated plasma plume did not directly touch the catalyst to avoid arcing and excessive heating induced by plasma. More information about the plasma jet and catalyst material used here can be found in [25, 26].

2.2 Gas phase and surface characterizations

The FTIR-based experimental platform is described in figure 1. The APPJ was fixed on one of the three viewports with a ceramic feedthrough to the reactor, and the orifice-to-catalyst bed distance was fixed at 5 mm. The effect of the plasma-to-catalyst distance is not the focus of this work and will not be discussed further. Note that the orifice-to-catalyst distance will affect the particle fluxes incident on the catalyst since plasma-generated species decay in the afterglow. This effect has been seen in prior work where the plasma-catalyst interaction was affected by orifice-to-catalyst distance [25, 26].

The gas species produced by the plasma catalysis reactions flowed into a home-made gas detection cell with a length of 15 cm, where the real-time gas phase measurement was performed by FTIR. The quantification of gas phase species was performed using Beer's law by converting IR absorbance obtained from the FTIR measurement to number density (number/cm³).

Operando surface characterization was performed by DRIFTS. Incident IR light went through the KBr windows on the reactor and was scattered at the catalyst surface and reflected to the detector, enabling to collect information from surface species. The density of surface species is qualitatively related to the IR absorbance acquired by DRIFTS [27]. Although we did not attempt to quantify the densities of surface species from DRIFTS data (see [27]), just the qualitative analysis of surface species provides valuable information on plasma-catalyst interactions. Complementary gas phase and surface characterizations are described in detail in [25, 26].

Before each experiment, the gas lines were evacuated to a pressure below 10⁻⁵ torr. The reactor and gas detection cell were purged by Ar flow to minimize the effect of impurities in the ambient environment, such as CO₂ and water vapor. For some experiments the catalyst bed was heated to 500 °C at a heating rate of 10 °C/min. Gas phase and surface characterizations were performed under application of plasma operated at different power levels. To investigate the effect of catalyst activation by plasma, different experimental process sequences were applied, and these are described in detail in section 3.2.

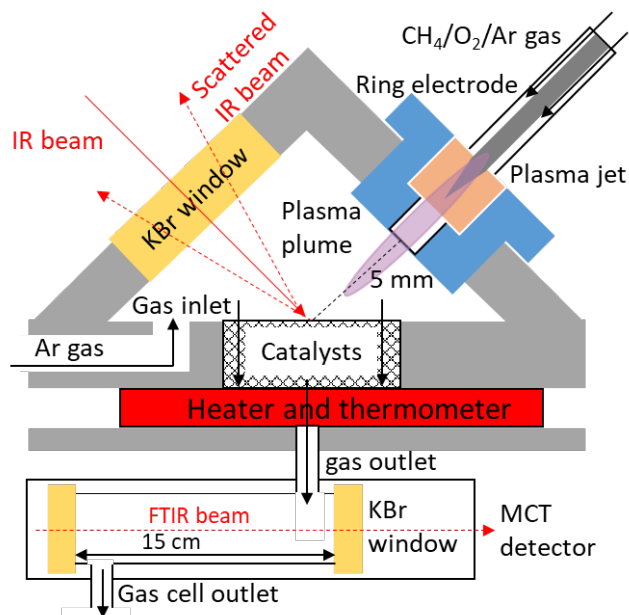


Figure 1. Schematic setup of the FTIR-based experimental platform integrated with the APPJ [25, 26].

3. Results and discussion

3.1 Comparison of product evolution when CH₄ flowed through the plasma as compared to downstream of APPJ

In previous work, CH₄ was injected downstream of the APPJ [25, 26] rather than directly being admitted to the plasma jet. Hence, entrainment of CH₄ into the ionized plasma plume, where interaction with high-energy electrons was possible, was required to break C-H bonds. For that gas flow configuration, the methane-plasma coupling was not efficient since most CH₄ diffused to the plasma effluent afterglow, where the high-energy electrons were depleted rapidly according to the non-Maxwellian properties of electron energy distribution function (EEDF) [28]. The limited CH₄-plasma plume interaction was especially pronounced when small plasma power levels were used and the plume was shorter in length. By flowing CH₄ directly through

the ionized plasma, strong CH₄ and plasma coupling took place and the CH₄ conversion rate was strongly enhanced. This is shown in figure 2 for catalyst temperatures of 25 °C or 500 °C.

Electron-impact dissociation of CH₄ to CH_n or vibrational excitation of CH₄ in the plasma region [16, 29] was prominent in this work, while the CH₄ activation by other species, e.g. atomic O and singlet O₂, is negligible [30]. At 500 °C, the CH₄ conversion is higher than at 25 °C, which can be explained by the plasma-catalyst synergy effect at elevated catalyst temperature [26]. Note that the thermally driven CH₄ conversion was negligible when compared to plasma-induced CH₄ oxidation for conditions where the CH₄ was directly flown through the plasma zone. The CO production is lower while the CO₂ yield is higher at 500 °C than at 25 °C. This is because CO is converted to CO₂ at elevated catalyst temperature, as we have found in previous experiments.

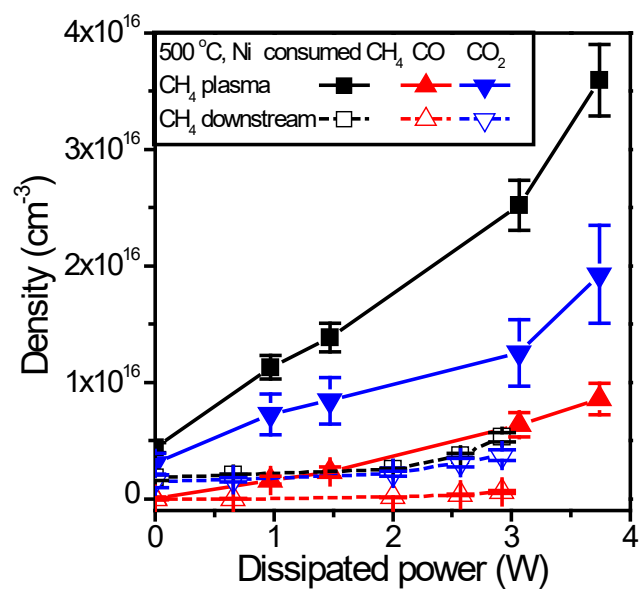
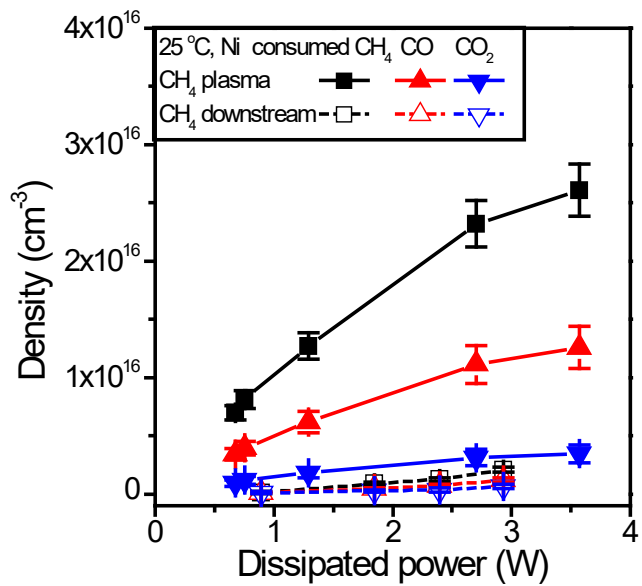


Figure 2. Comparison of CH₄ conversion between flowing CH₄ directly through the plasma jet and downstream of the plasma jet at a catalyst temperature of 25 °C (a) and 500 °C (b).

3.2. Activation of catalyst by APPJ

3.2.1 Comparison of APPJ with small and large powers

The real-time downstream gas phase and surface measurements of the nickel catalyst at 500 °C exposed to the APPJ with large and small dissipated powers revealed different results, as shown in figure 3. With 4 W plasma power, the CH₄ conversion was more intense than the one with 1 W plasma power, as indicated by more CH₄ consumption and CO and CO₂ production. The surface CO and CH_n were barely discernable from DRIFTS measurements in the case of 1 W plasma power. In contrast, large IR absorption due to surface CO and CH_n was observed using 4 W plasma power. The surface CH_n coverage was stable across different experiments, independent of plasma exposure time, whereas the surface CO coverage consistently increased. The oxidation of surface CH_n to surface CO likely accounts for the different behaviors of surface CO and CH_n. If the dehydrogenation of CH₄ to CH_n and the oxidation of surface CH_n to surface CO and other gas species is balanced, this can give rise to a stable surface CH_n coverage and consistent increase of surface CO, depending on the lifetime of CO on the surface. Note that at the beginning of plasma applications, the densities of consumed CH₄ and produced CO₂ gas and the abundance of surface CH_n rapidly increased and then gradually decayed until steady state was achieved, whereas the CO gas and surface CO did not show such a declining trend. We repeated these experiments multiple times and the response to plasma ignition was consistent. The differences in the evolution of the signals of different species might imply that they participate in different reaction pathways, and more work is required to clarify the mechanistic origin of this difference.

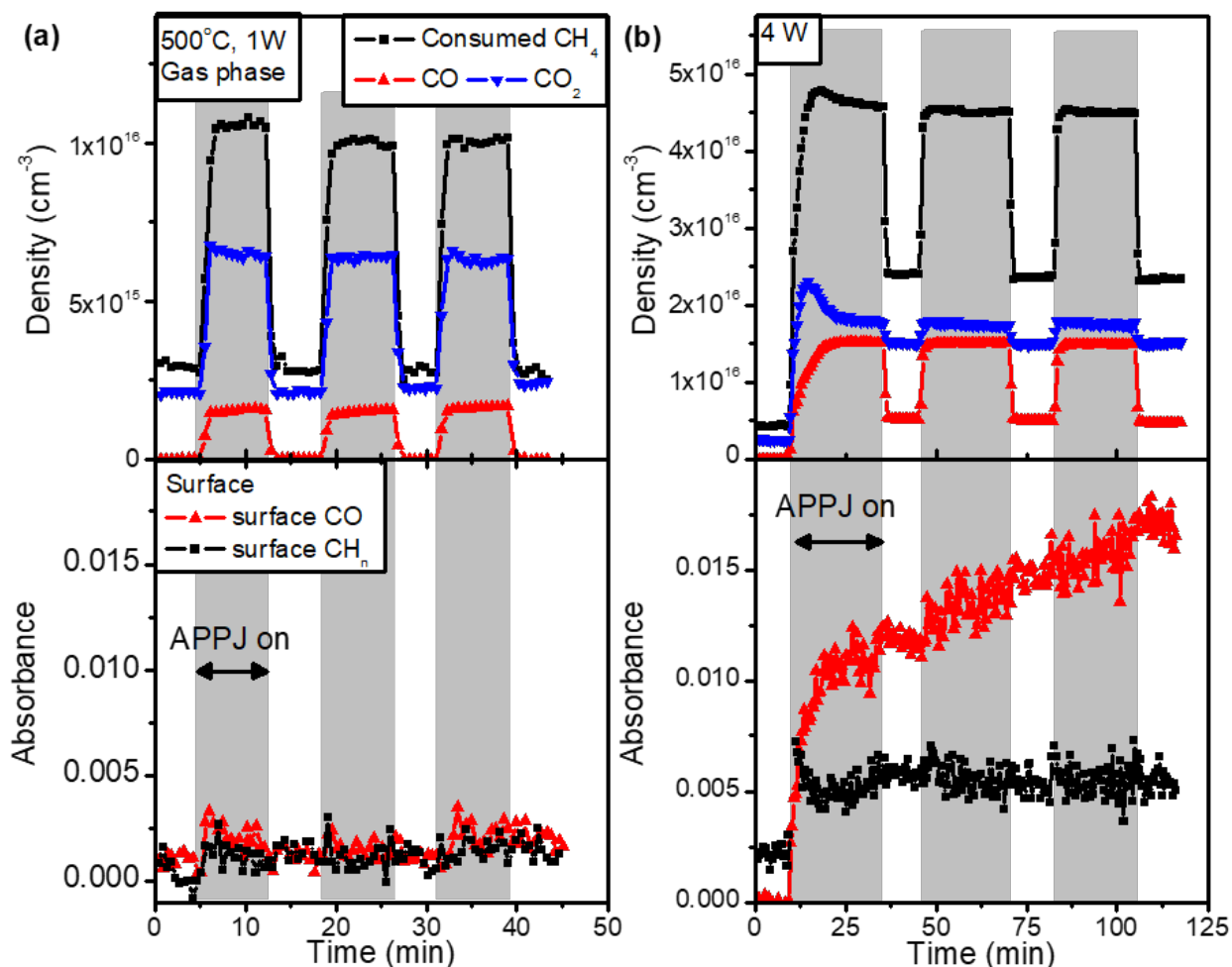


Figure 3. Comparison of CH₄ conversion by the APPJ using small power (1 W, figure a) and large power (4 W, figure b) levels at a catalyst temperature of 500 °C. The gas phase results are shown in the top graphs and the DRIFTS results are shown in the bottom graphs. The plasma treatment was applied three times to check repeatability.

Another discrepancy between using 1 W and 4 W plasma jet was the thermal catalytic reaction process after plasma exposure. Figure 3a shows that the thermal reaction after shutting off the 1 W plasma was similar to the initial thermal reaction, i.e., CH₄ was oxidized to CO₂ without the generation of gas phase CO. The thermal reaction after exposure of the nickel catalyst to the 4

W plasma showed important differences. First, the consumption of CH₄ and production of CO₂ gases were enhanced compared to the thermal reaction before the onset of plasma. Second, gas phase CO continued to be generated after the plasma had been extinguished. This indicates that the nickel catalyst was “activated” by exposure to the effluent of the APPJ operated at 4 W power. Prior to this, we did not observe CO generation using our nickel catalyst at 500 °C without plasma operation [25, 26]. Hu et al. [12, 31, 32] compared the unreduced and reduced nickel catalyst for thermally driven CH₄ oxidation and found that the CH₄ gas underwent complete oxidization by surface-adsorbed oxygen to produce CO₂ only using unreduced nickel catalyst at 500 °C. However, using pre-reduced nickel catalyst, CO gas was generated along with CO₂ at a catalyst temperature of 500 °C. Song et. al. [19] investigated the partial oxidation of CH₄ over a dielectric barrier discharge plasma and NiO catalyst and found that the NiO could be reduced to Ni. Dissanayake et al. [9] also did not detect CO formation using unreduced nickel catalyst at 500 °C, whereas after heating the catalyst to 750 °C, CO formation drastically increased. They used x-ray photoemission spectroscopy (XPS) to analyze the catalyst and found that the unreduced Ni interacted with the Al₂O₃ support at 750 °C which led to the formation of reduced Ni catalyst that catalyzed the partial oxidation of CH₄ to CO. Inelastic neutron scattering experiments performed by Barboun et. al. revealed that surface-adsorbed reactive N species produced in the plasma can further react with other gas phase species to enhance their dissociation and thermal reactions subsequently [33]. It is possible that a similar mechanism would apply to CH_n species in our case. Based on the comparison with the literature insights, the “catalyst activation” observed in our experiments may possibly be attributed to one or more of three mechanisms: (i) The reduction of catalyst through the interaction with CH₄ or CO

[17, 19]. (ii) The plasma may heat the nickel catalyst to a temperature above 750 °C, which would promote the formation of reduced Ni by the interaction between unreduced Ni and Al₂O₃ support. (iii) The reactive surface CH_n species could lower the activation energy, and thus keep the catalyst active and promote formation of CO gas.

Among these potential mechanisms, heating of the catalyst to a temperature of 750 °C or higher does not seem feasible. The gas temperature of a similar plasma jet fed with air and Ar was measured to be less than 120 °C [34]. The plasma jet utilized in this work was a remote plasma source that the plasma plume did not directly contact the catalyst surface. We measured the catalyst temperature increase due to heating by the APPJ effluent at the largest power level (~4 W) when at room temperature and found that this was only 15 °C, far less than the required 750 °C. This temperature increase became negligible when the catalyst was heated to 500 °C.

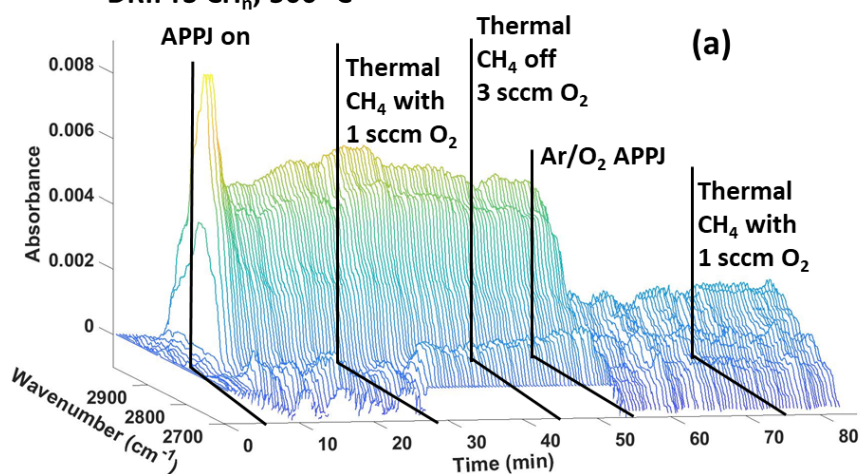
3.2.2 Investigation of the catalyst activation.

A higher oxygen flow rate to the APPJ can remove surface-adsorbed species [25] and even etch the polystyrene polymer thin films due to its high reactivity induced by the reactive species [35, 36]. To assess the importance of CH_n in the observed catalyst activation, O₂/Ar APPJ was applied to remove the surface CH_n and the thermal catalytic reaction was evaluated immediately after. The time-dependent DRIFTS spectra of surface CH_n and CO are displayed in three-dimensional waterfall graphs in figure 4a and b. As the 4 W CH₄/O₂/Ar plasma was ignited, the surface CH_n and CO absorption bands emerged. The CH₄ flow was then turned off and the O₂ flow was increased to 3 sccm, which enhanced the reactivity of the O₂/Ar APPJ.

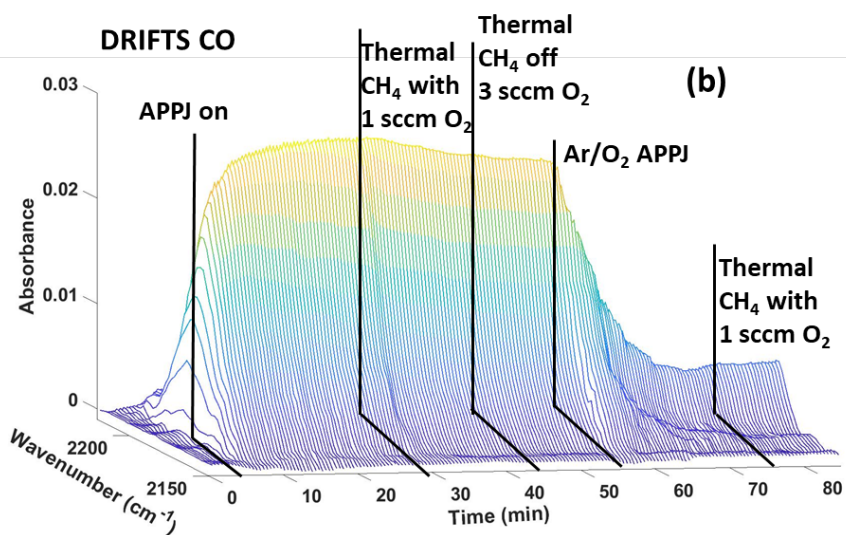
When the O₂/Ar plasma was ignited, the surface CH_n and CO were gradually removed. The surface CH_n was almost depleted while surface CO was still present at a low coverage after the treatment of O₂/Ar plasma. After the surface cleaning process, CH₄ with 1 sccm O₂ was reintroduced.

The evolution of the surface species located at 1900-1000 cm⁻¹ is also provided in figure 4c. During the ignition of CH₄/O₂/Ar plasma, absorption bands at 1590 cm⁻¹ (carboxylate [37, 38]), 1420 cm⁻¹ (C-O-H group [39] or CH₂ [40]), and 1280 cm⁻¹ (carbonate [41]) emerged, as the reaction took place. Upon the ignition of O₂/Ar plasma, the 1590 cm⁻¹ and 1420 cm⁻¹ bands decreased and the 1280 cm⁻¹ band did not show obvious changes due to exposure to the O₂/Ar plasma. The unambiguous assignment of the IR absorption bands in 1900-1000 cm⁻¹ is difficult and requires secondary experimental verification, and the detailed discussion of the species in this region is not the focus of this work.

DRIFTS CH_n, 500 °C



DRIFTS CO



1900-1000 cm⁻¹ region

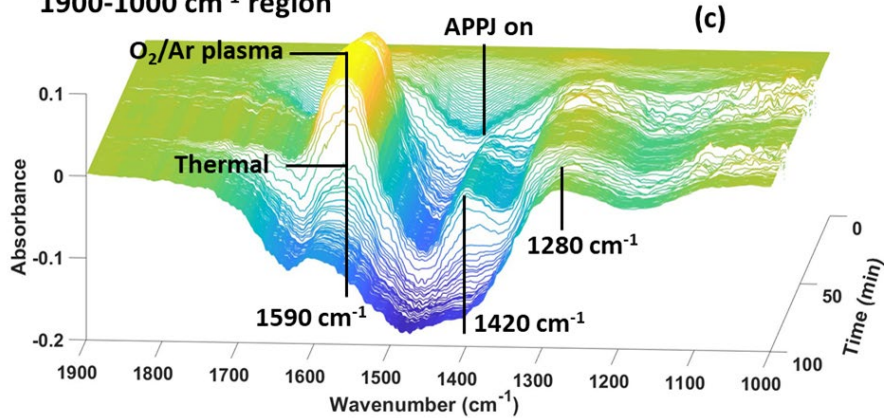


Figure 4. The time-dependent waterfall graphs of surface CH_n (a), surface CO (b) and the species located at $1900\text{-}1000\text{ cm}^{-1}$ (c) are shown to illustrate the response to the application of O_2/Ar plasma. The catalyst was initially activated by 4 W $\text{CH}_4/\text{O}_2/\text{Ar}$ plasma at $500\text{ }^\circ\text{C}$.

Following the same procedure, we performed downstream gas phase measurements to evaluate the thermal catalytic reactions after the exposure to O_2/Ar plasma and analyzed the gas phase and surface measurements together to evaluate the time dependence of these processes. As shown in figure 5a, after the removal of surface CH_n by O_2/Ar plasma, catalyst activation no longer existed. This is demonstrated by the low thermal reaction intensity and the fact that gas phase CO production is negligible compared to the enhanced formation rate seen for the purely thermal process after exposure to a high power $\text{Ar}/\text{CH}_4/\text{O}_2$ plasma. This observation seems consistent with the hypothesis that the surface CH_n is responsible for the catalyst activation. Alternatively, since flowing O_2 gas and exposure of the Ni catalyst to O_2/Ar plasma causes oxidation of the nickel even at room temperature, judging from experiments where Ni had been treated with O_2 gas flow [42, 43]. Hence, we cannot rule out the possibility that Ni catalyst activation was caused by reduction of the Ni catalyst.

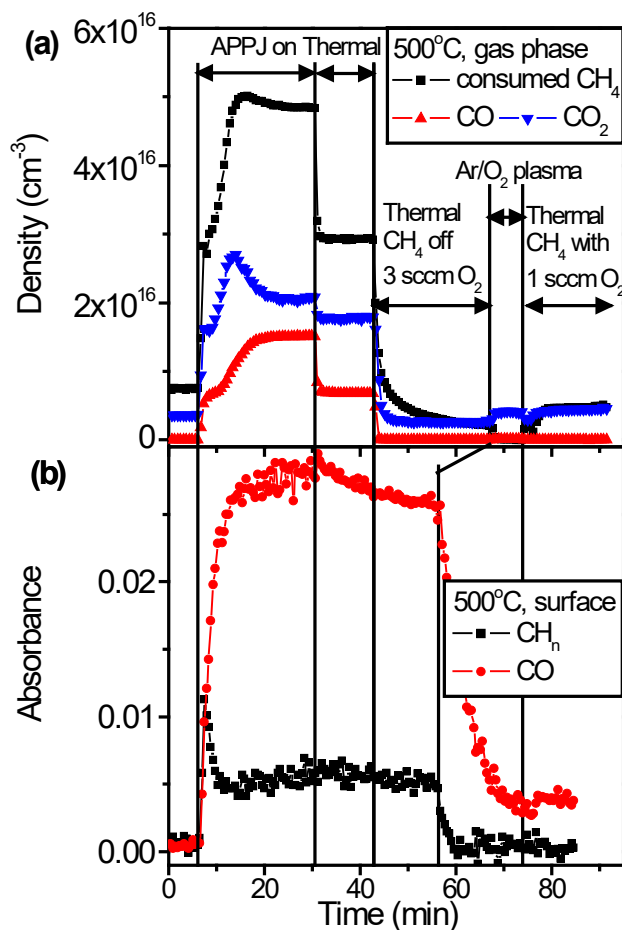


Figure 5. Time-dependent downstream gas phase (a) and surface DRIFTS measurements (b) of CH_4 conversion as catalyst was deactivated by O_2/Ar plasma at 500°C .

Turning off CH_4 flow and only flowing O_2 with Ar cannot remove the surface CH_n or CO, as illustrated in figures 4 and 5, where the absorption due to surface CO and CH_n did not change significantly after the CH_4 flow was shut off. In order to evaluate if the catalyst activation was due to the reduction of catalyst by interaction with plasma-produced species, e.g. vibrationally excited CH_4 , CH_n or CO species, rather than using O_2/Ar plasma to remove surface species, we performed a test in which we only turned off the CH_4 flow and continued the O_2 flow to evaluate whether this could oxidize the reduced catalyst if there was any. The results of

shutting the CH₄ flow are shown in figure 6. In figure 6a, after shutting off the CH₄ flow and exposing the catalyst to the O₂ flux for around 20 min, the once-activated catalyst was deactivated by the continued O₂ flow. This is indicated by the weak thermal reaction which also did not yield CO after reintroduction of the CH₄ flow. Since the surface CH_n and CO species were still present on the catalyst surface as the exposure to the O₂/Ar gas mixture flow took place, the deactivation of catalyst was likely due to the oxidation of the previously plasma-reduced nickel catalyst by the O₂ gas at elevated catalyst temperature.

We also exposed the catalyst to O₂ flux for a shorter time and expected that the activated catalyst should not be completely deactivated since not all the reduced Ni can be re-oxidized in a short time period under an O₂ flow. In figure 6b the following sequence is shown: After the catalyst was activated by plasma initially, we shut off the CH₄ flow and then exposed the catalyst to O₂/Ar flow for 3 minutes. The active catalyst was not completely deactivated during the short period of O₂ gas exposure, as indicated by the still-enhanced thermal reaction and the production of CO gas after reintroduction of the CH₄ flow. The finding that different results are seen when exposing the active catalyst to the O₂/Ar flow for different periods indicates that the reduction of nickel oxide to reduced Ni catalyst may be the reason for the thermal reaction enhancement and the production of CO gas without the application of plasma. This still requires direct confirmation, i.e. by confirming the reduction of the nickel catalyst by plasma operated at large power.

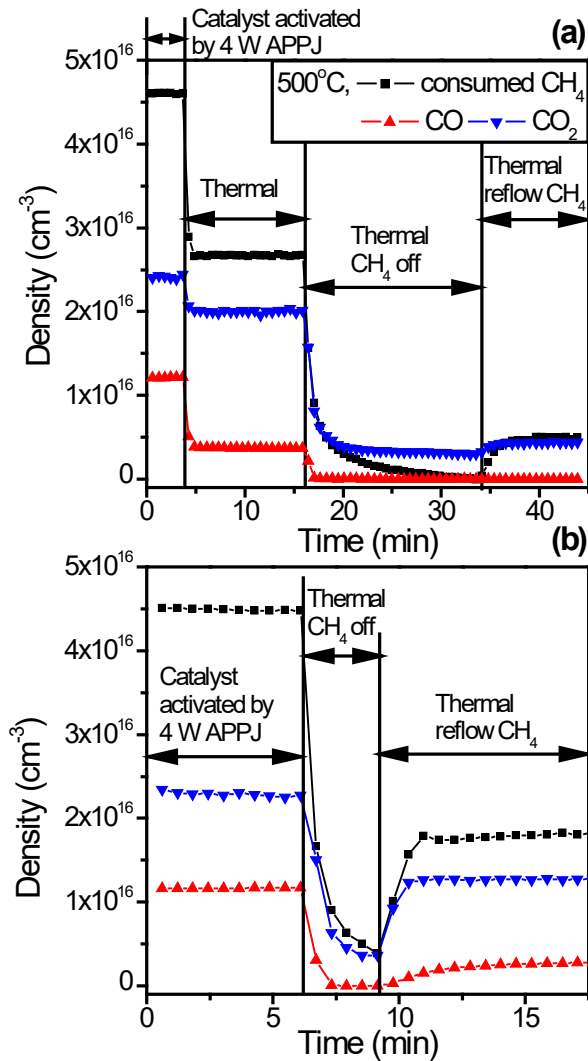


Figure 6. Downstream gas phase measurements showing the influence of shutting off the CH₄ flow for different periods on the magnitude of the thermally driven CH₄ conversion at a catalyst temperature of 500 °C. The activated catalyst was either exposed to O₂/Ar gas mixture for a long (~20 min, figure (a)) or a short (~3 min, figure (b)) period, respectively. The significant difference here is not only that the CH₄ flow is off for a longer time, but that the reduced catalyst is exposed to the oxidizing flux for a much longer time.

Figure 7 summarizes data measured for the CH₄, CO and CO₂ species density changes as a result of thermally activated reactions of the Ni catalyst for different conditions. The mild thermal

reaction before plasma exposure (labeled as 1) contrasted with the thermal reaction with catalyst activated by plasma (labeled as 2). More CH₄ reduction and CO₂ yield were measured for the latter, and CO generation was also observed. The identical results of the application of O₂/Ar plasma (labeled as 3), which additionally removed the surface CH_n and CO species, and just exposing the catalyst to O₂ flux (labeled as 4) implied that catalyst activation may not be due to the presence of reactive CH_n species on the catalyst surface. The catalyst activation was partially degraded when the activated catalyst was exposed to O₂ flow for a short time (~3 min, labeled as 5). This supports the hypothesis that the catalyst activation by APPJ is related to the reduction of the nickel catalyst, and such activation can be reversed by exposing the reduced catalyst to an oxidizing flux.

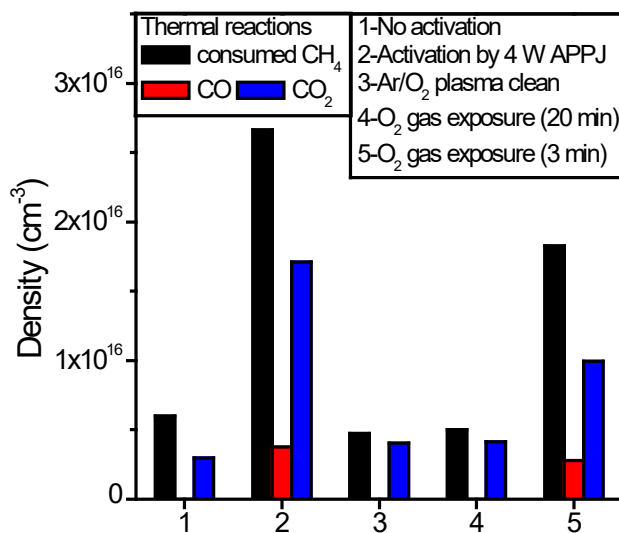


Figure 7. Comparison of thermal reactions under different conditions. 1- pure thermal reaction without plasma activation; 2- after plasma activation using 4 W CH₄/O₂/Ar plasma; 3- after deactivation of the Ni

surface by O₂/Ar plasma; 4- after deactivation by O₂ gas exposure for 20 min; 5- after partial deactivation by O₂ gas exposure for 3 min.

The thermal reaction enhancement by plasma modification of a catalyst surface seen here may be related to efforts where plasma is used to prepare thermal catalyst materials [24]. In the past, researchers mainly attributed the enhancement of the catalysis reaction by plasma to directly induced reactions in the plasma phase [44], enhanced surface reactions from incident plasma generated fluxes that includes reactive species like neutrals, photons, electrons and ions and that can act alone or in concert [5, 45], or the increase of catalyst temperature due to the absorption of plasma-generated heat [19]. This work provides a new perspective for reaction enhancement, where the plasma improves the efficacy of the catalyst by plasma-induced catalyst reduction, which will not take place for conventional thermally driven reactions unless much higher operating temperatures are used. This observation indicates that the mechanisms and potential benefits of plasma catalysis are widespread and may have broad applications.

3.3 Shifts of surface CO vibrational frequency

The vibrational frequency of surface CO from the DRIFTS measurement has a frequency of around 2190 cm⁻¹. The frequency of gas phase CO in our experiments has a vibrational frequency of 2143 cm⁻¹ as measured by FTIR [25, 26], in agreement with other work [46, 47]. Surface CO gives therefore rise to a blue shift of around 50 cm⁻¹. In addition, a systematic vibrational frequency shift of surface CO was observed in response to changes in plasma operation and catalyst temperature (figure 8 and 9). We believe that the analysis of the

observed CO frequency shifts by atomistic calculations may offer valuable mechanistic insights on plasma-catalyst interactions.

3.3.1 Effect of plasma on CO vibrational frequency

Figure 8a shows the surface CO spectra evolution in the catalyst activation experiments of figure 3. The surface CO absorbance increased with time and was explained by the oxidation of surface CH_n , as described in 3.2.1. The surface CO has an IR absorption band centered at 2185 cm^{-1} when the plasma was on. The band immediately shifted to 2189 cm^{-1} once the plasma was extinguished. Figure 8b is the time-dependent surface CO spectra of the experiments using O_2/Ar plasma to remove the surface CH_n and deactivate the catalyst. In figure 8b, the surface CO absorption band was located at 2185 cm^{-1} during the initial exposure to $\text{CH}_4/\text{O}_2/\text{Ar}$ plasma. When the plasma was turned off, the frequency shifted to 2189 cm^{-1} , in agreement with the observation shown in figure 8a. With the ignition of O_2/Ar plasma, the IR band shifted back to 2185 cm^{-1} while surface CO was removed gradually. Once the plasma was turned off, the CO IR band shifted to 2189 cm^{-1} again. These kinds of CO vibrational frequency shifts while fairly small, were consistently observed in repeated experiments and are reproducible.

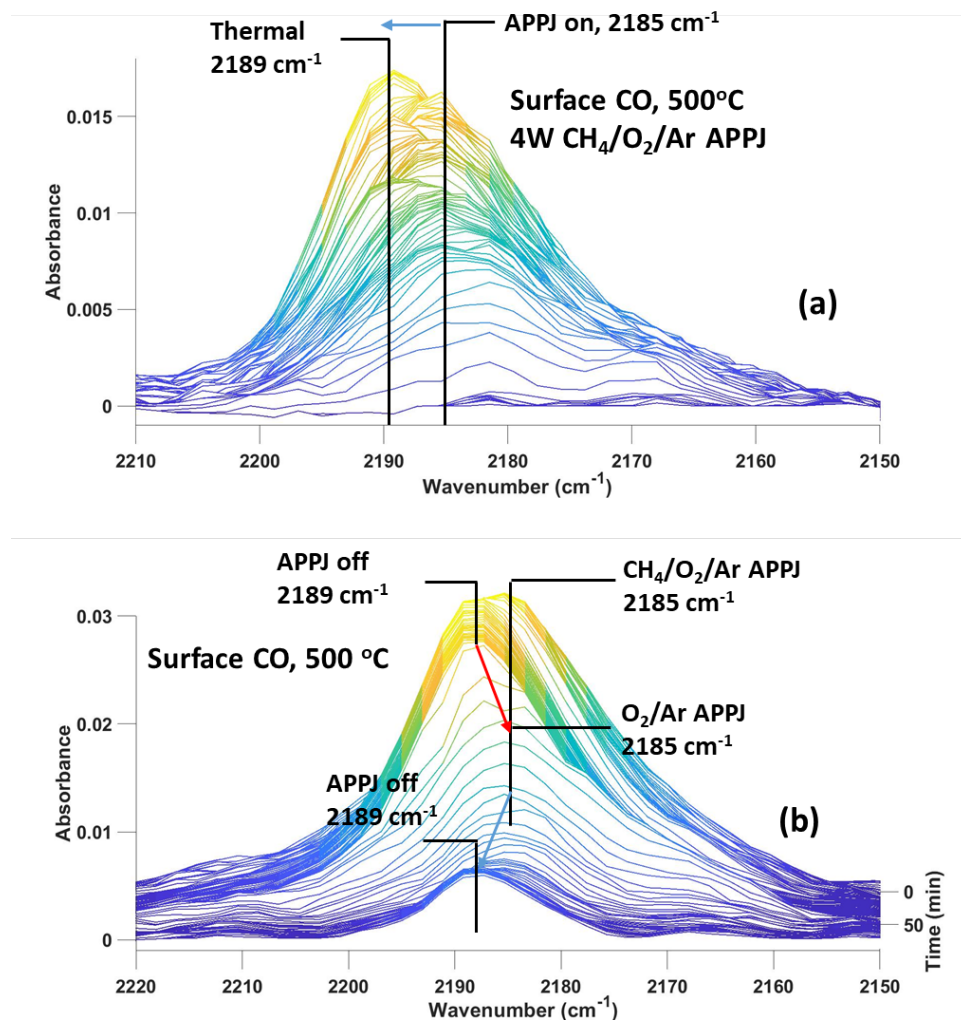


Figure 8. The effect of CH₄/O₂/Ar plasma (a) and O₂/Ar plasma (b) on surface CO IR spectra. The catalyst temperature is 500 °C.

3.3.2 Effect of catalyst temperature on CO vibrational frequency

We performed a temperature-programmed experiment to investigate the effect of catalyst temperature on surface CO vibrational frequency. The catalyst was heated from 100 °C to 500 °C at a rate of 10 °C/min. The time-dependent graph of the CO spectra is shown in figure 9.

Heating the catalyst caused a red shift of CO vibrational frequency from 2192 cm⁻¹ at a catalyst temperature of 100 °C to 2185 cm⁻¹ when heated to 500 °C. The surface CO coverage also

increased with temperature, which was likely due to the oxidation of surface CH_n , as illustrated in figure 10.

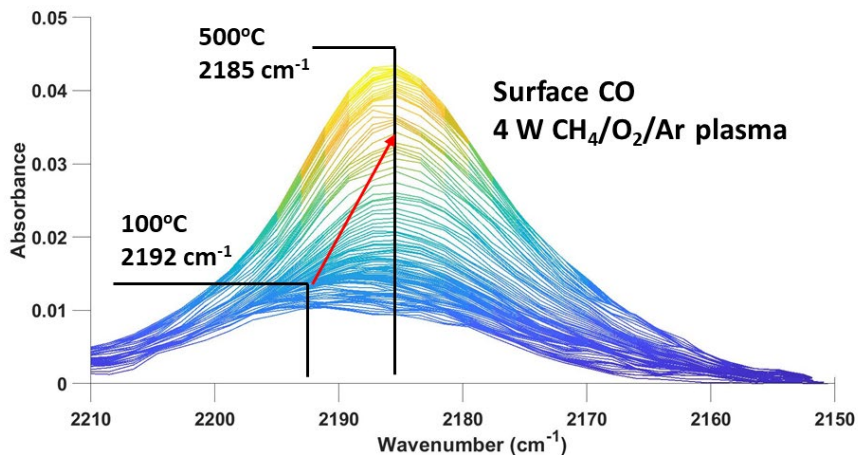


Figure 9. The effect of catalyst temperature on the IR frequency of surface CO while being exposed to the fluxes from a 4 W $\text{CH}_4/\text{O}_2/\text{Ar}$ plasma. The catalyst was heated from 100 °C to 500 °C at a rate of 10 °C/min

For the reader's reference, we have summarized the vibrational frequency of CO at different conditions measured by the FTIR in table 1.

Table 1. Summary of the CO vibrational frequency at different conditions

| Condition | Vibrational frequency (cm^{-1}) |
|---|--|
| Gas phase CO | 2143 |
| CO on 500 °C catalyst, no APPJ | 2189 |
| CO on 500 °C catalyst, $\text{CH}_4/\text{O}_2/\text{Ar}$ APPJ on | 2185 |
| CO on 500 °C catalyst, O_2/Ar APPJ on | 2185 |
| CO on 100 °C catalyst, $\text{CH}_4/\text{O}_2/\text{Ar}$ APPJ on | 2192 |

3.3.3 Possible explanations of surface CO vibrational frequency shift.

The literature indicates that the IR vibrational frequency of CO can be influenced by three major effects: mechanical renormalization, vibrational coupling, and electrostatic or chemical effect of the substrate [48]. The mechanical renormalization, also called wall effect, can account for the $\sim 50 \text{ cm}^{-1}$ blue shift of surface CO relative to gas phase CO [48, 49]. The change of the CO vibrational frequency arises from the repulsion of the surface CO stretch when adhered to a rigid substrate like nickel [49].

The electrostatic and chemical effect involves the charge transfer between the substrate material and the CO species [48]. By means of semi-empirical calculations, Politzer et al. [50] concluded that the C-O bond frequency was sensitive to the σ and π electronic charge transfer upon the formation of Ni-CO structure. The σ electrons from CO can transfer to the nickel surface, giving rise to a blue shift of CO bond, while the electron back-donation from the nickel surface to the antibonding $2\pi^*$ orbital in CO decreases the CO vibrational frequency. A substrate surface with more electron acceptors or electronegative elements, e.g. oxygen, decreases the electron back-donation to the CO, and results in a blue shift [51]. In contrast, a surface with higher electron density can enhance the electron back-donation [52]. As shown in figure 8, both $\text{CH}_4/\text{O}_2/\text{Ar}$ plasma and O_2/Ar plasma induce the same 4 cm^{-1} red shift compared to a non-plasma condition at a catalyst temperature of $500 \text{ }^\circ\text{C}$. These observations indicate that the frequency shift caused by the plasma is related to the intrinsic properties of APPJ that do not vary too much when different plasma feed gas combinations are used. By using Thomson scattering, Gessel et. al. [53] measured the electron density for an identical Ar plasma jet for different gas mixtures and found that the electron density did not vary too much. Electrons

produced in the plasma jet can be deposited on the catalyst surface, and consequently enhance the electron back-donation to the $2\pi^*$ antibonding orbital in surface CO, resulting in a red shift of the same scale. The fact that high-energy electrons decay rapidly in the far plasma effluent afterglow [54] makes the CO frequency a mild shift (4 cm^{-1}). Moreover, the electric field change on the catalyst surface induced by the plasma application can potentially shift the CO frequency, and such shifts may be related to the electric field strength [48, 55, 56]. The evaluation of the influence of plasma-induced electric field on the CO frequency requires the measurements and relative modeling of the electric field, which is out of the scope of this work.

Figure 9 shows that as the catalyst temperatures was raised, the CO coverage also increased. The increase of surface CO may be due to the oxidation of surface CH_n , as shown in figure 10. With the increase of catalyst temperature, the surface CH_n started to decrease at around $300\text{ }^\circ\text{C}$, and the surface CO started to increase simultaneously. According to [48], the surface coverage increases the surface CO frequency due to the enhancement of intermolecular dipole-dipole coupling and intermolecular repulsion with surface species occupation, which is contrary to our results. The CO frequency can increase by 40 cm^{-1} when the coverage increases from 0 to 0.5 [57]. However, the increase of surface CO coverage in figure 8a does not indicate an influence on CO frequency. The CO frequency shift observed in our experiments likely does not result from the change of surface CO coverage. According to [48, 58], as the substrate temperature increases, surface CO can diffuse from the ordered phase (island) to the disordered structure where the intermolecular distance is larger. This can explain the reduction of through-space intermolecular dipole coupling and results in a small blue shift. Another possibility is the uptake of surface oxygen through the reaction with CH_4 , CH_n or CO. The lower

oxygen content on the surface can stimulate electron back-donation and results in a red shift of CO vibrational frequency [51, 59].

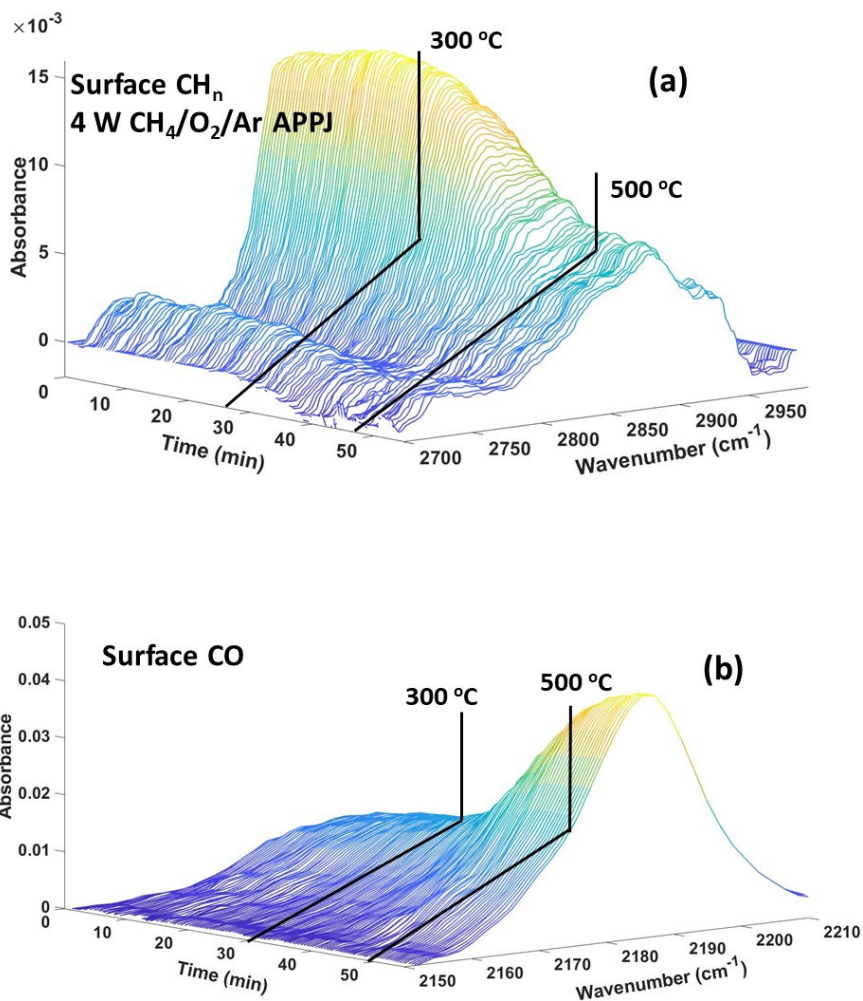


Figure 10. Temperature-dependent evolution of surface CH_n (a) and CO (b) with the application of 4 W CH₄/O₂/Ar plasma. The catalyst was heated from 100 °C to 500 °C at a rate of 10 °C/min.

We have provided several possible explanations for the observed CO vibrational frequency shift based on the study of the literature and our understanding of the CO-nickel catalyst structure. Other considerations can also cause the shift of CO vibrational frequency, e.g., image dipole

[48], the interaction with other surface species [59], etc. Our measurements are insufficient to allow a clear-cut determination of the reasons for the CO frequency shift. Nevertheless, our observations suggest a new methodology to study plasma-catalyst interactions through the changes of surface CO vibrational frequency for different plasma-catalyst operating and interaction conditions, and combining these with atomistic simulations. Extra efforts, such as expanding the experimental parameters, computational modeling, or modifying the intermolecular or surface species-catalyst vibrational coupling by isotopic exchange [60], may be helpful in understanding the mechanistic origin of the observed CO vibrational frequency shifts and how these may be related to plasma-catalyst interactions.

4. Conclusions

In this work, FTIR was applied to investigate the APPJ-enhanced CH₄ oxidation over a SiO₂/Al₂O₃ supported nickel catalyst. We compared two plasma feed gas configurations and found that directly flowing CH₄ through the plasma source was much more efficient in terms of CH₄ conversion than injecting CH₄ downstream of the plasma and interacting it with the effluent of Ar/O₂ fed to the plasma source. By exposing the Ni catalyst to plasma fluxes created at higher power levels, catalyst activation was observed. Here catalyst activation signifies a thermal reaction after plasma exposure of the catalyst that became more intense as compared to before plasma exposure, and additionally for which CO production at 500°C was consistently observed even if the plasma was extinguished, whereas CO production was absent for a purely thermally driven reaction at 500 °C for a Ni catalyst without prior plasma treatment. By application of O₂/Ar plasma or by just exposing an activated catalyst to a flowing O₂/Ar gas

mixture for an extended time, deactivation of the activated catalyst took place. The exposure of the activated Ni catalyst surface to O₂/Ar gas did not remove the surface CH_n, but can oxidize the reduced nickel catalyst. This suggests that catalyst activation is likely not due to reactive surface CH_n for the conditions studied here, but may be related to the reduction of nickel catalyst. However, at this time we have no direct spectroscopic evidence in support of this statement. DRIFTS measurements of surface CO species revealed a consistent shift of the CO IR vibrational frequency that could be induced by plasma operation, and systematic shifts were also seen when the catalyst temperature was varied. The atomistic interpretation of these observations may be a promising approach to gain new perspectives on plasma-catalyst interactions by using surface species as a local probe and interpreting the spectroscopic information in terms of physical models.

5. Acknowledgments

We acknowledge the financial support of the National Science Foundation (CBET-1703211) and US Department of Energy (DE-SC0020232). We thank Dr. Shiqiang Zhang, Jingkai Jiang, Dr. Peter Bruggeman, Frank Doherty, Dr. Bryan Goldsmith, Dr. Pingshan Luan, Dr. Andrew Knoll, Kang-Yi Lin and Sang-Jin Chung for helpful discussions and collaborations on aspects of this work.

References

1. Tendero, C., et al., *Atmospheric pressure plasmas: A review*. Spectrochimica Acta Part B: Atomic Spectroscopy, 2006. **61**(1): p. 2-30.
2. Kogelschatz, U., *Dielectric-barrier discharges: Their history, discharge physics, and industrial applications*. Plasma Chemistry and Plasma Processing, 2003. **23**(1): p. 1-46.
3. Luan, P., et al., *Decontamination of raw produce by surface microdischarge and the evaluation of its damage to cellular components*. Plasma Processes and Polymers, 2019. **16**(5): p. 1800193.
4. Whitehead, J.C., *Plasma-catalysis: the known knowns, the known unknowns and the unknown unknowns*. Journal of Physics D: Applied Physics, 2016. **49**(24): p. 243001.
5. Mehta, P., et al., *Overcoming ammonia synthesis scaling relations with plasma-enabled catalysis*. Nature Catalysis, 2018. **1**(4): p. 269-275.
6. Pou, J.O., C. Colominas, and R. Gonzalez-Olmos, *CO₂ reduction using non-thermal plasma generated with photovoltaic energy in a fluidized reactor*. Journal of Co₂ Utilization, 2018. **27**: p. 528-535.
7. Mei, D.H., S.Y. Liu, and X. Tu, *CO₂ reforming with methane for syngas production using a dielectric barrier discharge plasma coupled with Ni/gamma-Al₂O₃ catalysts: Process optimization through response surface methodology*. Journal of Co₂ Utilization, 2017. **21**: p. 314-326.
8. Tu, X., et al., *Dry reforming of methane over a Ni/Al₂O₃ catalyst in a coaxial dielectric barrier discharge reactor*. Journal of Physics D-Applied Physics, 2011. **44**(27).
9. Dissanayake, D., et al., *PARTIAL OXIDATION OF METHANE TO CARBON-MONOXIDE AND HYDROGEN OVER A Ni/AL₂O₃ CATALYST*. Journal of Catalysis, 1991. **132**(1): p. 117-127.
10. Hu, Y.H. and E. Ruckenstein, *Catalytic conversion of methane to synthesis gas by partial oxidation and CO₂ reforming*, in *Advances in Catalysis, Vol 48*, B.C. Gates and H. Knozinger, Editors. 2004. p. 297-345.
11. Prettre, M., C. Eichner, and M. Perrin, *The catalytic oxidation of methane to carbon monoxide and hydrogen*. Transactions of the Faraday Society, 1946. **42**(0): p. 335b-339.
12. Hu, Y.H. and E. Ruckenstein, *Isotopic GCMS Study of the Mechanism of Methane Partial Oxidation To Synthesis Gas*. The Journal of Physical Chemistry A, 1998. **102**(51): p. 10568-10571.
13. Kim, H.-H., A. Ogata, and S. Futamura, *Oxygen partial pressure-dependent behavior of various catalysts for the total oxidation of VOCs using cycled system of adsorption and oxygen plasma*. Applied Catalysis B: Environmental, 2008. **79**(4): p. 356-367.
14. Brune, L., et al., *Dry reforming of methane via plasma-catalysis: influence of the catalyst nature supported on alumina in a packed-bed DBD configuration*. Journal of Physics D-Applied Physics, 2018. **51**(23).
15. Goujard, V., J. Tatibouet, and C. Batiot-Dupeyrat, *Influence of the Plasma Power Supply Nature on the Plasma-Catalyst Synergism for the Carbon Dioxide Reforming of Methane*. IEEE Transactions on Plasma Science, 2009. **37**(12): p. 2342-2346.
16. Nozaki, T., et al., *Dissociation of vibrationally excited methane on Ni catalyst: Part 1. Application to methane steam reforming*. Catalysis Today, 2004. **89**(1): p. 57-65.
17. Pietruszka, B., K. Anklam, and M. Heintze, *Plasma-assisted partial oxidation of methane to synthesis gas in a dielectric barrier discharge*. Applied Catalysis a-General, 2004. **261**(1): p. 19-24.
18. Heintze, M. and B. Pietruszka, *Plasma catalytic conversion of methane into syngas: the combined effect of discharge activation and catalysis*. Catalysis Today, 2004. **89**(1-2): p. 21-25.

19. Song, L.J., Y.L. Kong, and X.H. Li, *Hydrogen production from partial oxidation of methane over dielectric barrier discharge plasma and NiO/gamma-Al₂O₃ catalyst*. International Journal of Hydrogen Energy, 2017. **42**(31): p. 19869-19876.
20. Wang, Z., et al., *Catalyst Preparation with Plasmas: How Does It Work?* ACS Catalysis, 2018. **8**(3): p. 2093-2110.
21. Sheng, Z., et al., *Oxidation behavior of Ni/Al₂O₃ catalyst in nonthermal plasma-enabled catalysis*. Journal of Physics D: Applied Physics, 2018. **51**(44): p. 445205.
22. Wang, L., et al., *Plasma driven ammonia decomposition on a Fe-catalyst: eliminating surface nitrogen poisoning*. Chemical Communications, 2013. **49**(36): p. 3787-3789.
23. Mei, D., et al., *Plasma-assisted conversion of CO₂ in a dielectric barrier discharge reactor: understanding the effect of packing materials*. Plasma Sources Science and Technology, 2014. **24**(1): p. 015011.
24. Zhang, S. and G.S. Oehrlein, *From thermal catalysis to plasma catalysis: a review of surface processes and their characterizations*. Journal of Physics D: Applied Physics, 2021. **54**(21): p. 213001.
25. Zhang, S., et al., *Mechanistic aspects of plasma-enhanced catalytic methane decomposition by time-resolved operando diffuse reflectance infrared Fourier transform spectroscopy*. Journal of Physics D-Applied Physics, 2020. **53**(21).
26. Knoll, A.J., et al., *Infrared studies of gas phase and surface processes of the enhancement of catalytic methane decomposition by low temperature plasma*. Journal of Physics D-Applied Physics, 2019. **52**(22).
27. Sirita, J., S. Phanichphant, and F.C. Meunier, *Quantitative analysis of adsorbate concentrations by diffuse reflectance FT-IR*. Analytical Chemistry, 2007. **79**(10): p. 3912-3918.
28. Trenchev, G., S. Kolev, and Z. Kiss'ovski, *Modeling a Langmuir probe in atmospheric pressure plasma at different EEDFs*. Plasma Sources Science & Technology, 2017. **26**(5).
29. Goujard, V., et al., *Plasma-assisted partial oxidation of methane at low temperatures: numerical analysis of gas-phase chemical mechanism*. Journal of Physics D-Applied Physics, 2011. **44**(27).
30. Nozaki, T., et al., *Selective conversion of methane to synthetic fuels using dielectric barrier discharge contacting liquid film*. Journal of Physics D: Applied Physics, 2011. **44**(27): p. 274010.
31. Hu, Y.H. and E. Ruckenstein, *Broadened Pulse-Step Change-Isotopic Sharp Pulse Analysis of the Mechanism of Methane Partial Oxidation to Synthesis Gas*. The Journal of Physical Chemistry B, 1998. **102**(1): p. 230-233.
32. Hu, Y.H. and E. Ruckenstein, *Multiple Transient Response Methods To Identify Mechanisms of Heterogeneous Catalytic Reactions*. Accounts of Chemical Research, 2003. **36**(10): p. 791-797.
33. Barboun, P.M., et al., *Inelastic Neutron Scattering Observation of Plasma-Promoted Nitrogen Reduction Intermediates on Ni/gamma-Al₂O₃*. ACS Energy Letters, 2021: p. 2048-2053.
34. Gaens, W.V., P.J. Bruggeman, and A. Bogaerts, *Numerical analysis of the NO and O generation mechanism in a needle-type plasma jet*. New Journal of Physics, 2014. **16**(6): p. 063054.
35. Luan, P. and G.S. Oehrlein, *Interaction of long-lived reactive species from cold atmospheric pressure plasma with polymers: Chemical modification by ozone and reactive oxygen-nitrogen species*. Journal of Vacuum Science & Technology A, 2019. **37**(5): p. 051303.
36. Knoll, A.J., et al., *Polymer etching by atmospheric-pressure plasma jet and surface micro-discharge sources: Activation energy analysis and etching directionality*. Plasma Processes and Polymers, 2018. **15**(5): p. 1700217.
37. Stere, C., et al., *A design of a fixed bed plasma DRIFTS cell for studying the NTP-assisted heterogeneously catalysed reactions*. Catalysis Science & Technology, 2020. **10**(5): p. 1458-1466.
38. Stere, C.E., et al., *Probing a Non-Thermal Plasma Activated Heterogeneously Catalyzed Reaction Using in Situ DRIFTS-MS*. ACS Catalysis, 2015. **5**(2): p. 956-964.

39. Marikhin, V.A., et al., *IR spectra of long-chain alpha,omega-alkanediols: 1,22-docosanediol and 1,44-tetratetracontanediol*. Polymer Science Series A, 2008. **50**(4): p. 403-410.
40. Yao, X., et al., *Structure investigation of β -D-fructose crystal under high pressure: Raman scattering, IR absorption, and synchrotron X-ray diffraction*. Journal of Molecular Structure, 2020. **1220**: p. 128746.
41. Vayssilov, G.N., et al., *Reassignment of the Vibrational Spectra of Carbonates, Formates, and Related Surface Species on Ceria: A Combined Density Functional and Infrared Spectroscopy Investigation*. The Journal of Physical Chemistry C, 2011. **115**(47): p. 23435-23454.
42. Lambers, E.S., et al., *Room-temperature oxidation of Ni(110) at low and atmospheric oxygen pressures*. Oxidation of Metals, 1996. **45**(3): p. 301-321.
43. Flege, J.I., et al., *Self-limited oxide formation in Ni(111) oxidation*. Physical Review B, 2011. **84**(11): p. 115441.
44. Nair, S.A., T. Nozaki, and K. Okazaki, *In situ fourier transform infrared (FTIR) study of nonthermal-plasma-assisted methane oxidative conversion*. Industrial & Engineering Chemistry Research, 2007. **46**(11): p. 3486-3496.
45. Rouwenhorst, K.H.R., H.H. Kim, and L. Lefferts, *Vibrationally Excited Activation of N₂ in Plasma-Enhanced Catalytic Ammonia Synthesis: A Kinetic Analysis*. ACS Sustainable Chemistry & Engineering, 2019. **7**(20): p. 17515-17522.
46. Rothman, L.S., et al., *The HITRAN2012 molecular spectroscopic database*. Journal of Quantitative Spectroscopy & Radiative Transfer, 2013. **130**: p. 4-50.
47. Huber, K., *Molecular Spectra and Molecular Structure: IV. Constants of Diatomic Molecules*. 2013: Springer US.
48. Hoffmann, F.M., *Infrared reflection-absorption spectroscopy of adsorbed molecules*. Surface Science Reports, 1983. **3**(2): p. 107-192.
49. Pacchioni, G., G. Cogliandro, and P.S. Bagus, *Characterization of oxide surfaces by infrared spectroscopy of adsorbed carbon monoxide: a theoretical investigation of the frequency shift of CO on MgO and NiO*. Surface Science, 1991. **255**(3): p. 344-354.
50. Politzer, P. and S.D. Kasten, *An investigation of the high-frequency form of carbon monoxide chemisorbed on nickel oxide*. Surface Science, 1973. **36**(1): p. 186-194.
51. Lu, Y., et al., *Origin of the High CO Oxidation Activity on CeO₂ Supported Pt Nanoparticles: Weaker Binding of CO or Facile Oxygen Transfer from the Support?* ChemCatChem, 2020. **12**(6): p. 1726-1733.
52. Kubota, J., et al., *Self-modification of Ni Metal Surfaces with CeO₂ to Suppress Carbon Deposition at Solid Oxide Fuel Cell Anodes*. Fuel Cells, 2017. **17**(3): p. 402-406.
53. Gessel, B.v., R. Brandenburg, and P. Bruggeman, *Electron properties and air mixing in radio frequency driven argon plasma jets at atmospheric pressure*. Applied Physics Letters, 2013. **103**(6): p. 064103.
54. Gaens, W.V. and A. Bogaerts, *Kinetic modelling for an atmospheric pressure argon plasma jet in humid air*. Journal of Physics D: Applied Physics, 2013. **46**(27): p. 275201.
55. Pacchioni, G. and P.S. Bagus, *Point-charge effects on the vibrational frequency of CO chemisorbed on Cu and Pd clusters: A model for CO with ionic coadsorbates*. Physical Review B, 1989. **40**(9): p. 6003-6011.
56. Luo, J.S., R.G. Tobin, and D.K. Lambert, *Electric field screening in an adsorbed layer: CO on Pt(111)*. Chemical Physics Letters, 1993. **204**(5): p. 445-450.
57. Ortega, A., F.M. Huffman, and A.M. Bradshaw, *The adsorption of CO on Pd(100) studied by IR reflection absorption spectroscopy*. Surface Science, 1982. **119**(1): p. 79-94.
58. Pfnür, H., et al., *High resolution vibrational spectroscopy of CO on Ru(001): The importance of lateral interactions*. Surface Science, 1980. **93**(2): p. 431-452.

59. Kim, C.M., C.W. Yi, and D.W. Goodman, *CO–NO and CO–O₂ Interactions on Cu(100) between 25 and 200 K Studied with Infrared Reflection Absorption Spectroscopy*. *The Journal of Physical Chemistry B*, 2005. **109**(5): p. 1891-1895.
60. Escalona Platero, E., S. Colluccia, and A. Zecchina, *Dipole coupling and chemical shifts in CO overlayers adsorbed on NiO*. *Surface Science*, 1986. **171**(3): p. 465-482.